ChemComm

Cite this: *Chem. Commun.*, 2012, **48**, 6484–6486

www.rsc.org/chemcomm

COMMUNICATION

Hydrogen evolution across nano-Schottky junctions at carbon supported MoS_2 catalysts in biphasic liquid systems†

Peiyu Ge,[a] Micheál D. Scanlon,[a] Pekka Peljo,[b] Xiaojun Bian,[c] Heron Vubrel,[d] Arlene O'Neill,[e] Jonathan N. Coleman,[e] Marco Cantoni,[f] Xile Hu,[d] Kyösti Kontturi,[b] BaoHong Liu[c] and Hubert H. Girault*[a]

Received 24th February 2012, Accepted 11th May 2012
DOI: 10.1039/c2cc31398g

The activities of a series of MoS_2-based hydrogen evolution catalysts were studied by biphasic reactions monitored by UV/Vis spectroscopy. Carbon supported MoS_2 catalysts performed best due to an abundance of catalytic edge sites and strong electronic coupling of catalyst to support.

Molybdenum disulphide (MoS_2) has been rigorously characterized by experimental and computational means as an alternative electrocatalyst to Pt-group metals towards the Hydrogen Evolution Reaction (HER, *i.e.* $2H^+ + 2e^- \rightarrow H_2$). MoS_2 reduces protons at low overpotentials *via* under co-ordinated sulphur edge sites, while its basal planes remain catalytically inert.[1] The primary factors that influence electrocatalytic activity are catalyst morphology and electrical conductivity. Nanocrystalline MoS_2 is much more active than catalytically inert bulk MoS_2 due to the exposure of more reactive sulphur edge sites.[1] In turn, exfoliated MoS_2, *i.e.* two-dimensional MoS_2 nanosheets,[2] should also show enhanced catalytic activity due to a further increase in these sites. Recently, the syntheses of MoS_2 on reduced graphene oxide sheets and MoS_2 on mesoporous carbon have been achieved by the groups of Dai[3] and Liu,[4] respectively. Strong chemical coupling and interactions between Mo precursors and functional groups on graphene oxide or mesoporous carbon allowed the nucleation and selective growth of highly disperse MoS_2 nanoparticles (NPs), free of aggregation, on both substrates. However, in the absence of either substrate, identical experimental procedures to the original syntheses produced much larger coalesced MoS_2 particles. The lower overpotentials for the HER, for both electrocatalysts, were attributed to the intimate interconnections between the conductive substrates and MoS_2 NPs. This interaction allowed the formation of smaller and more disperse MoS_2 NPs, thereby unleashing an abundance of accessible catalytic edge sites, and ensuring a robust electrical coupling of MoS_2 to the underlying carbon supports with rapid electron transfer from the less-conducting MoS_2 NPs to the electrode.[3,4]

The interface between two immiscible electrolyte solutions (ITIES) represents a soft platform to develop new water splitting, *i.e.* artificial photosynthetic, protocols.[5] Protons can be reduced at these defect free soft electrified interfaces to produce H_2 in the presence of organic reducing agents such as cobaltocene[6] or decamethylferrocene (DMFc)[5,7] in the organic phase. Previously, we have catalyzed this process by the *in situ* reduction of metallic salts, forming adsorbed metallic NPs of Pt or Pd,[7e] or by adsorbing MoS_2 particles at the ITIES.[7d]

Herein, the relative abilities of nanocrystalline MoS_2, exfoliated MoS_2, and MoS_2 NPs grown on either graphene or mesoporous carbon particles were investigated as hydrogen evolution catalysts (HECs) at the ITIES (for synthesis and characterisation details of each catalyst see Section S1, ESI†). The lipophilic tetrakis (pentafluorophenyl)borate anion (TB^-) in the aqueous phase (w) acts both as a proton pump, leading to the extraction of HTB acid to the organic phase (o), 1,2-dichloroethane (1,2-DCE), and as a potential determining ion to polarise the liquid–liquid interface.[5]

$$H^{+,w} + TB^{-,w} \rightarrow HTB^{o} \qquad (1)$$

The reaction between DMFc and aqueous protons catalyzed by MoS_2-based particles can be written as a proton transfer reaction followed by its reduction in the organic phase[7a,d]

$$DMFc^{o} + H^{+,o} \xrightarrow{\text{catalyst in 1,2-DCE}} DMFc^{+,o} + \tfrac{1}{2}H_2 \qquad (2)$$

or as an interfacial reaction

$$DMFc^{o} + H^{+,w} \xrightarrow{\text{interfacial catalyst}} DMFc^{+,o} + \tfrac{1}{2}H_2 \qquad (3)$$

The concentrations of $DMFc^+$ formed during biphasic reactions in the presence and absence of different MoS_2-based

[a] *Laboratoire d'Electrochimie Physique et Analytique (LEPA), Ecole Polytechnique Fédérale de Lausanne (EPFL), Station 6, CH-1015 Lausanne, Switzerland. E-mail: Hubert.Girault@epfl.ch; Fax: +41 693 3667; Tel: +41 693 3145*
[b] *Department of Chemistry, Aalto University, P.O. Box 16100, 00076, Finland*
[c] *Department of Chemistry, Institute of Biomedical Sciences, Fudan University, Shanghai, 200433, P.R. China*
[d] *Laboratory of Inorganic Synthesis and Catalysis (LISC), EPFL, BCH-3305, CH-1015 Lausanne, Switzerland*
[e] *School of Physics and Centre for Research on Adaptive Nanostructures and Nanodevices (CRANN), Trinity College Dublin, D2, Ireland*
[f] *Interdisciplinary Centre for Electron Microscopy (CIME), EPFL, Station 12, CH-1015, Lausanne, Switzerland*

† Electronic supplementary information (ESI) available: Synthesis and characterisation of each MoS_2-based catalyst; experimental details, discussion and figures for UV/Vis, zeta (ζ)-potential, cyclic voltammetry experiments; MoS_2 band calculations. See DOI: 10.1039/c2cc31398g

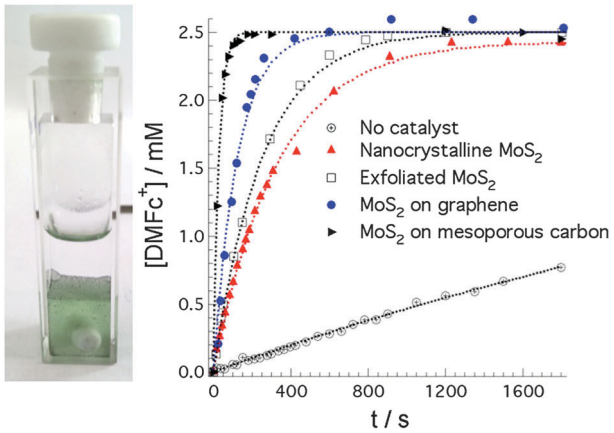

Fig. 1 Kinetics of the hydrogen evolution reaction (HER), in the absence and presence of each of the MoS_2-based catalysts, as followed by monitoring changes in the UV/Vis absorbance (λ_{max} = 779 nm) for $DMFc^+$. Fits (dotted lines) were obtained from the calculated rate constants (k/s^{-1}, see Table 1). On the left, a photograph of the two-phase reaction after 30 minutes stirring in an UV/Vis quartz cuvette sealed with a Teflon cap. The clear aqueous phase contains 10 mM LiTB and 100 mM HCl with 0.25 mM of MoS_2 particles visible at the interface; the green 1,2-DCE phase contains 2.5 mM $DMFc^+$ post reaction.

catalysts (0.25 mM) were monitored by observing changes of the UV/Vis absorbance at 779 nm (Fig. 1, for experimental details see Section S2, ESI†). The maximum stoichiometric amount of $DMFc^+$ (2.5 mM) limited by the initial DMFc concentration (2.5 mM) was attained after 1800 s in the presence of each catalyst. Slower kinetics in the absence of catalyst preclude the reaction from proceeding to completion during this time-frame. The reaction was found to be 1st order with respect to DMFc (Fig. S2, ESI†). The rate constants (Table 1) were calculated by fitting (Section S2, ESI†).

MoS_2 on mesoporous carbon particles were found to be the best catalyst for H_2 evolution, increasing the rate of reaction by a factor of 170. MoS_2 on graphene particles showed a 40 times increase in reaction rate, and exfoliated MoS_2 was slightly more effective compared to nanocrystalline MoS_2. These trends in the relative performances of each of the MoS_2-based particles to act as HECs were further corroborated by cyclic voltammetry (CV) studies at a potentiostatically polarised ITIES. For experimental details and a thorough discussion of the ion-transfer events refer to Section S3 (ESI†).

An increased abundance of exposed negatively charged sulphur edge atoms, as discussed, is expected on moving from nanocrystalline to exfoliated MoS_2 and on modifying the surfaces of graphene and mesoporous carbon particles with disperse islands of MoS_2. Directly measuring the surface

Table 1 Calculated apparent rate constants (k/s^{-1}) for the biphasic reaction, and the rate constant relative to the experiment without any catalyst ($k/k_{no\ catalyst}$)

Catalyst	k/s^{-1}	$k/k_{no\ catalyst}$
No catalyst	0.00021	1
Nanocrystalline MoS_2	0.0030	14
Exfoliated MoS_2	0.0039	19
MoS_2 on graphene	0.0080	38
MoS_2 on mesoporous carbon	0.036	171

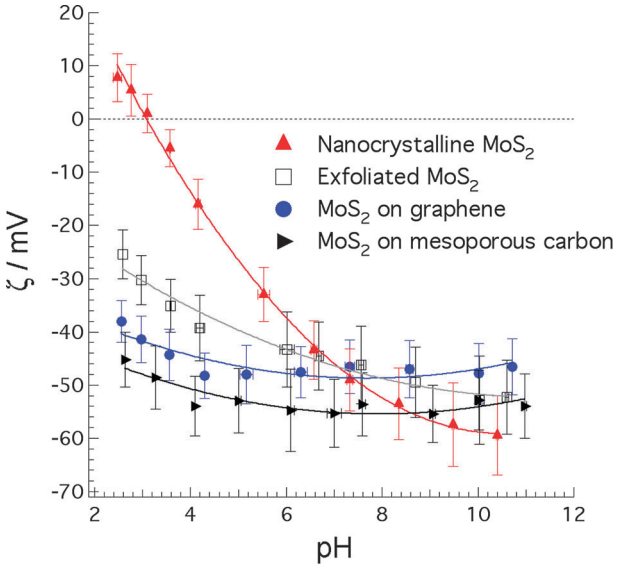

Fig. 2 Zeta (ζ)-potentials (mV) of nanocrystalline MoS_2, exfoliated MoS_2, MoS_2 on graphene and MoS_2 on mesoporous carbon as a function of pH in aqueous dispersions at concentrations of 0.7–1 mg per 5 ml.

charge of a particle for real systems is not possible. Instead, the zeta (ζ)-potential, *i.e.* the electrostatic potential difference between an average point at the hydrodynamic shear plane and the bulk liquid, may be probed and represents a measure of the surface charge.[8] Herein, the ζ-potential represents a useful qualitative probe to verify the relative abundances of sulphur edge sites for each electrocatalyst. The ζ-potential of each of the MoS_2-based catalysts was analysed using a Nano ZS Zetasizer (Malvern Instruments, U.K.) with irradiation (λ = 633 nm) from a He–Ne laser (Fig. 2, for experimental details and additional discussion see Section S4, ESI†). Substantial negative surface charges at pHs < 7 and shifts of the isoelectric points (pIs) below pH 2 were observed, on moving from nanocrystalline (pI $\approx$ 3.1)[9] to exfoliated MoS_2 and on modifying the surfaces of graphene and mesoporous carbon particles with disperse islands of MoS_2 (for ζ-potentials of the control materials, see Fig. S5, ESI†). More negative ζ-potentials over the pH range 2.5 to 11 for MoS_2 NPs grown on mesoporous carbon rather than on graphene particles infer the presence of more MoS_2 sulphur edge sites on mesoporous carbon, correlating with its superior rate of reaction as seen in Fig. 1.

A reaction scheme outlining the biphasic mechanism of proton reduction by DMFc in 1,2-DCE under anaerobic conditions, with carbon supported MoS_2 catalysts present either at the interface or in the bulk, is illustrated in Scheme 1 (see Section S5 (ESI†) for band calculations, redox potentials, *etc.*). An interfacial Galvani potential difference ($\Delta_o^w\phi$) is established due to the distribution of the lipophilic anion, TB^-. Consequently, protons are pumped across the interface and, in the presence of an MoS_2 species, are adsorbed at catalytic sulphur edge sites (denoted here as *). When the semiconductor MoS_2 is in contact with graphene (or, indeed, mesoporous carbon) an insulated nano-Schottky junction is formed, as highlighted in Scheme 1. For MoS_2 on graphene particles, electrons are transferred from graphene to the semiconductor until the Fermi levels are equalised. On transfer of

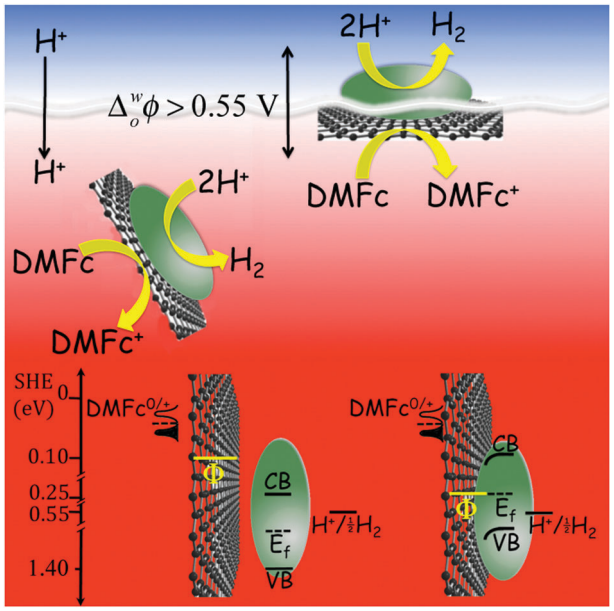

Scheme 1 Biphasic mechanism of proton reduction to molecular hydrogen in the presence of MoS_2 on graphene catalyst. $\Delta_o^w\phi$ is the interfacial Galvani potential difference established by distribution of the lipophilic anion, TB^-. VB and CB are the valence and conduction bands of MoS_2, respectively, E_f is the Fermi level of MoS_2 and Φ is the work function of graphene. The aqueous and organic phases are coloured blue and red, respectively.

an electron from graphene to MoS_2, the Fermi level of graphene is lowered. Inversely, since MoS_2 becomes negatively charged, the Fermi level moves up. Band bending occurs as a result of the excess negative charge transferring from graphene to MoS_2. DMFc is insoluble in the aqueous phase and electron injection can be considered to take place exclusively in 1,2-DCE. Electrons are injected from DMFc to a state in graphene close to the Fermi level. Next, the electrons transfer to an empty state in the conduction band of MoS_2 and, finally, electron transfer occurs to an adsorbed hydrogen atom at a catalytic edge site (H*). This results in the release of molecular hydrogen through one of the two processes: either $2H^* \rightarrow H_2 + 2^*$ or $H^+ + e^- + H^* \rightarrow H_2 + *$.[1a] From a thermodynamic point of view, only protons with sufficiently positive reduction potentials may be reduced. Protons present in the organic phase meet this criteria with a reduction potential of 0.55 V.[7a] Energetically, aqueous protons may also be reduced in the presence of a positive interfacial Galvani potential difference greater than 0.55 V.

The Gibbs energy of an adsorbed hydrogen (H*) on nanocrystalline MoS_2 edge sites is similar to that on Pt, *i.e.* close to zero.[1a] Thus, protonation and subsequent H_2 release occurs at an accelerated rate on MoS_2 compared to a mechanism without catalyst.[7c] Exfoliated MoS_2 is more reactive than nanocrystalline MoS_2, as more edge sites are exposed due to its graphene-like sheet structure, though the increase in the HER rate was not as substantial as expected (see Table 1). This observation may be due to exfoliated MoS_2 being present as many multilayers clumped together as particles and not as individual single-layer flakes. The conductive carbon supports increase the HER rate in multiple ways. Firstly, these supports act as nucleation sites for the formation of small and highly dispersed MoS_2 NPs, thus massively increasing the abundance of catalytic edge sites in comparison to nanocrystalline MoS_2 freely grown in solution.[3,4] Secondly, their conductive nature allow electron injection from DMFc to occur at any point on the hybrid catalyst, *i.e.* not specifically at the MoS_2 edge sites, increasing the cross-section of reaction between DMFc and the catalyst and hence also the reaction rate. The sizable increase in rate for MoS_2 on mesoporous carbon particles over its graphene analogue suggests that the very large specific surface area of mesoporous carbon allows huge loadings of small, highly dispersed MoS_2 NPs (hence more catalytic edge sites) than possible on the surface of comparatively flat graphene.

In conclusion, MoS_2 NPs nucleated and grown on carbon supports, in particular mesoporous carbon, act as superior electrocatalysts towards the HER. Their catalysis of the biphasic reduction of protons at the liquid–liquid interface offers new opportunities in energy research towards the development of artificial photosynthetic systems.

This work was financially supported by the SNF program "Solar fuels". The work in LSCI is supported by a ERC starting grant under the European Community's 7th Framework Programme (FP7 2007-2013)/ERC Grant agreement no. 257096. P.P. and K.K. acknowledge financial support from the Academy of Finland (Grant No. 133261).

Notes and references

1 (*a*) B. Hinnemann, P. G. Moses, J. Bonde, K. P. Jørgensen, J. H. Nielsen, S. Horch, I. Chorkendorff and J. K. Nørskov, *J. Am. Chem. Soc.*, 2005, **127**, 5308–5309; (*b*) T. F. Jaramillo, K. P. Jørgensen, J. Bonde, J. H. Nielsen, S. Horch and I. Chorkendorff, *Science*, 2007, **317**, 100–102; (*c*) J. Bonde, P. G. Moses, T. F. Jaramillo, J. K. Norskov and I. Chorkendorff, *Faraday Discuss.*, 2009, **140**, 219–231; (*d*) D. Merki, S. Fierro, H. Vrubel and X. Hu, *Chem. Sci.*, 2011, **2**, 1262–1267.
2 J. N. Coleman, M. Lotya, A. O'Neill and S. D. Bergin, *et al.*, *Science*, 2011, **331**, 568–571.
3 Y. Li, H. Wang, L. Xie, Y. Liang, G. Hong and H. Dai, *J. Am. Chem. Soc.*, 2011, **133**, 7296–7299.
4 X. Bian, J. Zhu, L. Liao, M. D. Scanlon, P. Y. Ge, C. Ji, H. H. Girault and B. H. Liu, 2012, in preparation.
5 M. A. Mendez, R. Partovi-Nia, I. Hatay, B. Su, P. Ge, A. Olaya, N. Younan, M. Hojeij and H. H. Girault, *Phys. Chem. Chem. Phys.*, 2010, **12**, 15163–15171.
6 U. Koelle, P. P. Infelta and M. Graetzel, *Inorg. Chem.*, 1988, **27**, 879–883.
7 (*a*) I. Hatay, B. Su, F. Li, R. Partovi-Nia, H. Vrubel, X. Hu, M. Ersoz and H. H. Girault, *Angew. Chem., Int. Ed.*, 2009, **48**, 5139–5142; (*b*) B. Su, I. Hatay, P. Y. Ge, M. Mendez, C. Corminboeuf, Z. Samec, M. Ersoz and H. H. Girault, *Chem. Commun.*, 2010, **46**, 2918–2919; (*c*) B. Su, I. Hatay, F. Li, R. Partovi-Nia, M. A. Méndez, Z. Samec, M. Ersoz and H. H. Girault, *J. Electroanal. Chem.*, 2010, **639**, 102–108; (*d*) I. Hatay, P. Y. Ge, H. Vrubel, X. Hu and H. H. Girault, *Energy Environ. Sci.*, 2011, **4**, 4246–4251; (*e*) J. J. Nieminen, I. Hatay, P. Ge, M. A. Mendez, L. Murtomaki and H. H. Girault, *Chem. Commun.*, 2011, **47**, 5548–5550.
8 A. V. Delgado, F. González-Caballero, R. J. Hunter, L. K. Koopal and J. Lyklema, *Pure Appl. Chem.*, 2005, **77**, 1753–1805.
9 S. M. Ahmed, *Electrochim. Acta*, 1982, **27**, 707–712.